Computations of Projectile Magnus Effect at Transonic Velocities

C. J. Nietubicz,* W. B. Sturek,† and K. R. Heavey‡
U.S. Army Ballistic Research Laboratory, Aberdeen Proving Ground, Maryland

A combined computational and experimental research program has been ongoing to develop a predictive capability for the Magnus effect that develops on spinning projectiles at angle of attack. This effort has been very successful in the supersonic regime and has now been extended to the transonic regime. Utilizing the time-marching, thin-layer, Navier-Stokes computational technique, flowfield solutions have been obtained for a spinning, 6-caliber-long, ogive-cylinder-boattail shape at Mach 0.91 and 2-deg angle of attack. The computed results predict the correct development of the Magnus force along the body; and comparisons between the computational results and experiment are encouraging. Details of the flowfield solution, such as turbulent boundary-layer velocity profiles and surface pressure distributions, are presented. The surface pressure and viscous shear components of the Magnus effect are presented as a function of axial position. A complete set of aerodynamic coefficients has been determined from the flowfield solutions. The computations for this research effort were obtained using a CDC 7600 and a Cray 1S computer.

Nomenclature

a = speed of sound
A = reference area, $\pi D^2/4$
c_p = specific heat (at constant pressure)
C_p = pressure coefficient
C_N = normal force coefficient, $\iint p_W \cos\phi \cos\theta_B \, dS/qA$
C_Y = Magnus force coefficient, $C_{Y_u} + C_{Y_w} + C_{Y_{p_w}}$
$C_{Y_{P_W}}$ = $\iint p_w \sin\phi \cos\theta_B dS/qA$
C_{Y_u} = $\iint \tau_x \sin\phi \sin\theta_B \, dS/qA$
C_{Y_w} = $\iint \tau_\phi \cos\phi \cos\theta_B \, dS/qA$
D = body diameter, 57.15 mm
$\hat{E},\hat{F},\hat{G}$ = flux vectors of transformed Navier-Stokes equations
M = Mach number
P = pressure, normalized by $\rho_\infty a_\infty^2$
$\hat{q}$ = vector of dependent variables
q = freestream dynamic pressure
R = body radius
Re = Reynolds number, $\rho_\infty D a_\infty/\mu_\infty$
Re_D = Reynolds number, $\rho_\infty D u_\infty/\mu_\infty$
S = surface area
$\hat{S}$ = viscous flux vector
t = physical time
u,v,w = Cartesian velocity components, normalized by a_∞
U,V,W = contravariant velocity components, normalized by a_∞
x,y,z = physical Cartesian coordinates
α = angle of attack
θ_B = local body slope
ξ,η,ζ = transformation coordinates in axial, circumferential, and radial directions
ρ = density, normalized by ρ_∞
τ = transformed time
τ_x = longitudinal wall shear stress
τ_ϕ = circumferential wall shear stress
ϕ = circumferential angle
ω = angular velocity, rev/s

Superscripts and Subscripts

$( )^*$ = critical value
$( )_\infty$ = freestream conditions

Presented as Paper 83-0224 at the AIAA 21st Aerospace Sciences Meeting, Reno, Nev., Jan. 10-13, 1983; received July 19, 1983; revision received Aug. 21, 1984. This paper is declared a work of the U.S. Government and therefore is in the public domain.

*Aerospace Engineer, Aerodynamics Research Branch, Launch and Flight Division. Member AIAA.
†Aerospace Engineer, Aerodynamics Research Branch, Launch and Flight Division. Associate Fellow AIAA.
‡Mathematician, Aerodynamics Reseach Branch, Launch and Flight Division.

Introduction

THE accurate prediction or experimental determination of projectile aerodynamics is of significant importance in the aerodynamic design of a shell. Accurate aerodynamic performance data are required early in the design of a projectile. In order to provide the needed performance data, a research effort has been ongoing to develop a sophisticated aerodynamic predictive capability. Early work had focused on the supersonic flight regime and, in particular, on the accurate prediction of the Magnus force. The Magnus force, which is very small in magnitude (on the order of one-tenth of the normal force), is a critical parameter in determining the dynamic stability of a shell. The Magnus force is generated by a spin-induced distortion of the boundary layer; therefore, correct modeling of the viscous/inviscid interaction is critical for accurate computations. The early work of Sturek et al.[1] showed that accurate results in the supersonic regime could be obtained for ogive-cylinder projectile shapes using a technique that involved separate computations of the turbulent boundary layer and the outer inviscid flowfield. As the projectile shapes were generalized to include boattails, more sophisticated computational techniques had to be employed. These new methods, which solved the parabolized, thin-layer, Navier-Stokes equations, were successfully applied to ogive-cylinder-boattail shapes by Schiff and Sturek.[2,3] The solution of the Navier-Stokes equations allows for the simultaneous computation of the viscous/inviscid flowfield and thus provides for improved physical modeling.

A region of critical aerodynamic behavior occurs in the transonic regime, $0.90 < M < 1.15$, where aerodynamic coefficients have been found to increase by as much as 100%. This flight velocity regime is both experimentally and computationally difficult. Thus, only a small amount of experimental

data is available for design studies and only limited computational studies have been made.

A time-marching procedure is required for transonic flow computations due to information propagating upstream. Thus, the parabolized Navier-Stokes (space-marching) approach cannot be used. An initial attempt to develop a computational capability suitable for Magnus prediction at transonic velocities was made by Nietubicz et al.,[4] whereby the thin-layer Navier-Stokes computational technique was applied to standard and hollow projectile shapes at 0-deg angle of attack. Computational results were also obtained for nonspinning projectiles at angle of attack[5]; however, limitations of computer resources (CDC 7600) became apparent. The computational results obtained by Deiwert[6] on the ILLIAC IV, in predicting the complicated flow pattern which exists on a boattailed afterbody, demonstrate the capability of the Navier-Stokes codes given sufficient computer resources. In this paper, recent results are presented for Magnus force computations using the Cray 1S computer. Comparisons are made with earlier CDC computer results and are further compared to some limited experimental data. A brief discusion of the numerical technique is included.

Governing Equations and Computational Technique

The Navier-Stokes equations solved herein make use of the thin-layer approximation.[7] That is, the viscous terms involving velocity gradients in both the longitudinal and circumferential directions are neglected. The viscous terms are retained, however, for velocity gradients in a direction nearly normal to the surface where large flowfield gradients exist. This formulation retains the momentum equations in all three coordinate directions. The retention of the three momentum equations allows for the computation of separated flow and thus differs significantly from boundary-layer assumptions.

The equations solved here are written in a generalized coordinate system. This allows a wide variety of body shapes to be computed using the same basic numerical technique. The notation for the physical and transformed coordinate systems is shown in Fig. 1. The three-dimensional, transformed, thin-layer Navier Stokes equations, written in nondimensional, strong conservation law form, are[8]

$$\partial_\tau \hat{q} + \partial_\xi \hat{E} + \partial_\eta \hat{F} + \partial_\zeta \hat{G} = Re^{-1} \partial_\zeta \hat{S} \qquad (1)$$

The general coordinate transformations are defined as

$\xi = \xi(x,y,z,t)$ longitudinal coordinate
$\eta = \eta(x,y,z,t)$ circumferential coordinate
$\zeta = \zeta(x,y,z,t)$ near-normal coordinate
$\tau = t$ time

The vector $\hat{q}$ contains the dependent variables (ρ, ρu, ρv, ρw, e). The flux vectors $\hat{E}$, $\hat{F}$, and $\hat{G}$ contain terms which arise from the conservation of mass, momentum, and energy in the three coordinate directions. The viscous terms are contained in the vector $\hat{S}$ which is seen to have variation in the ζ direction only. This represents the thin-layer approximation mentioned earlier. A more detailed description of the equations can be found in Ref. 8.

Equation (1) is written in transformed coordinates; therefore, the various body shapes are introduced through determination of the metric terms ξ_x, η_x, ζ_z, etc. These terms are formed by a combination of the derivative terms x_ξ, y_ξ, z_ξ, etc., and, together with the transformation Jacobian, allow for variable body geometries. Thus, one of the first steps in performing a computation is the generation of a computational grid which provides the x, y, and z points for the metric determination. These points are determined prior to the computations and are not changed with time. Examples of the computational grid used in this study are shown in Figs. 2 and 3. A two-dimensional slice of the overall grid is shown in Fig. 2. These grids were generated using a hyperbolic grid generation code described in Ref. 9. The upstream, downstream, and outer flowfield computational boundaries extended approximately 18 body diameters from the body surface. At this distance, the flowfield should be uniform and the imposed freestream boundary conditions are valid. Figure 3 shows an expanded view near the body. The clustering of grid points near the body surface is required to resolve the viscous components of the flowfield

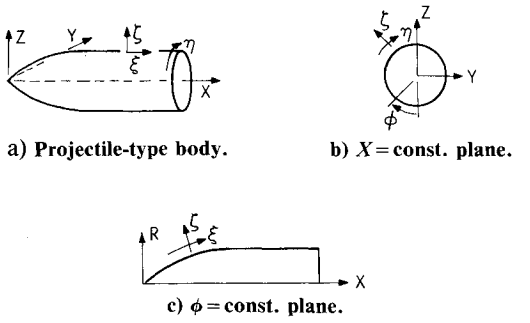

a) Projectile-type body. b) X = const. plane.

c) ϕ = const. plane.

Fig. 1 Physical and transformed coordinate system.

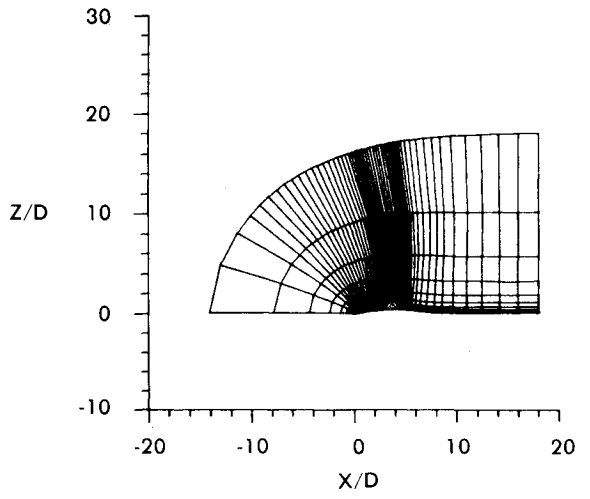

Fig. 2 Physical grid, total flowfield.

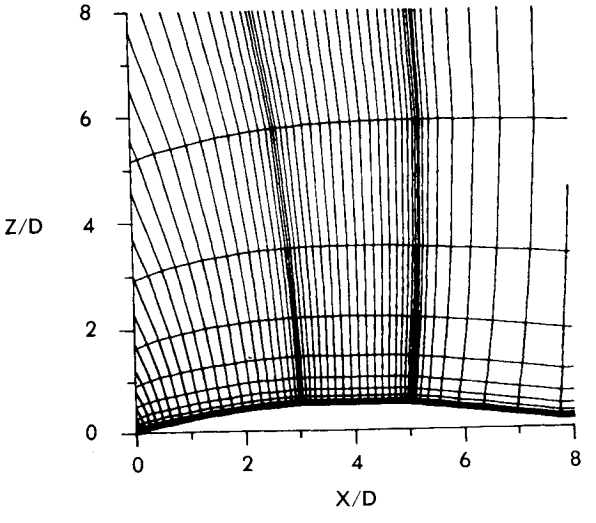

Fig. 3 Physical grid, expanded view near projectile surface.

near the body surface. Due to the lack of sufficient computer storage, judicious use must be made of the limited grid points available. In regions where the viscous effects are not predominant and the flowfield changes slowly, the grid points are sparse. Additional grid clustering is used in the longitudinal direction where significant flowfield gradients are expected. The two-dimensional grid shown in Fig. 2 was rotated about the body axis in 10-deg increments for the Cray computations (20-deg increments for the CDC 7600) to obtain the three-dimensional grid required for computations at angle of attack. The wake region was modeled by extending the boattail for approximately two calibers ($X/D=7.8$) then turning the grid line parallel to the model axis and extending it to the downstream boundary.

As mentioned in the Introduction, the Magnus effect is produced by a spin-induced distortion of the boundary layer. Therefore, the computation must be fully three dimensional since no plane of symmetry exists. The boundary conditions used for the computations are:

1) Inner boundary, body surface: $U=W=0$; $V=\omega D/a_\infty$; ρ is a first-order extrapolation; and p is calculated using the three transformed momentum equations.

2) Outer boundary: Constant freestream values are used for all variables.

3) Downstream boundary: $M<1$, pressure is fixed at p_∞ and all other variables are extrapolated; $M\geq 1$, first-order extrapolation on all variables.

4) Upstream axis line: All variables are extrapolated.

The numerical scheme used for the solution of Eq. (1) is a fully implicit, approximately factored, finite difference algorithm in delta form as analyzed by Beam and Warming.[10] This scheme can be first- or second-order accurate in time and second- or fourth-order accurate in the three spatial directions. The solution of the three-dimensional equations is implemented by an approximate factorization which allows the system of equations to be solved in three one-dimensional steps. This procedure has been utilized in previous applications[2-6] with a high degree of success. Additional details of the numerical method, computational algorithm, and boundary conditions can be found in Ref. 8.

The turbulence model employed is an algebraic eddy-viscosity model as developed by Baldwin and Lomax.[7] This same model has yielded excellent results for Magnus effects at supersonic velocities.[3]

As indicated in Eq. (1), this solution technique involves solving the time-dependent, thin-layer, Navier-Stokes equations. The procedure is started by assuming a uniform freestream solution for all grid points in the computational domain. A slow start of the boundary conditions is implemented and the calculation marches in time until a steady-state solution is obtained. A criterion for convergence is for the solution residual to decrease by three orders of magnitude. Also, the surface pressure distribution is checked for time invariance. The implicit technique used here allows for large computational time steps to be taken, which helps to reduce the total computation time.

Model Geometry and Experiment

One means of establishing the computational accuracy of a numerical scheme is through comparisons with available experimental data. The model used for the experiment and computational study presented here is an idealization of a realistic artillery projectile geometry. The experimental model shown in Fig. 4 consists of a three-caliber (1 caliber = maximum body diameter), sharp, secant-ogive nose, a two-caliber cylindrical midsection, and a one-caliber 7-deg conical afterbody or boattail. A similar model was used for the computational studies with the only difference being a 5% rounding of the nose tip. The nose-tip rounding was done for computational efficiency and is considered to have little impact on the final integrated forces.

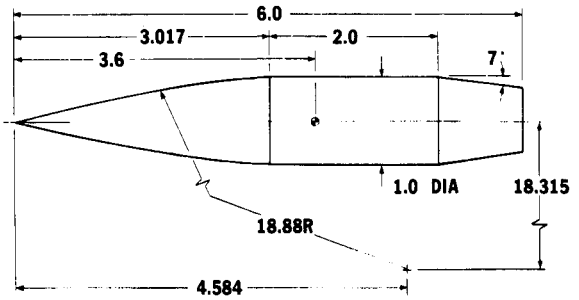

Fig. 4 Model details.

The surface pressure experimental data[11] used for comparison in this paper were obtained in the NASA Langley 8-ft Pressure Tunnel. The test conditions of 1 atm supply pressure and 320 K supply temperature resulted in a Reynolds number of 4.5×10^6 based on model length. The model was instrumented with pressure ports at 15 longitudinal stations. Pressure data were obtained at Mach numbers of 0.91 to 1.2 and angles of attack from 0 to 10 deg. The pressure data were obtained with the model nonspinning.

Additional tests[12] were conducted at the Naval Surface Weapons Center for similar tunnel conditions. This test utilized a different model with the same geometry which now included the capability for spin. Magnus force and moment measurements were obtained while the model coasted down to zero spin after spinning to 500 rev/s. Aerodynamic force measurements were obtained at Mach 0.91 for α = 0-10 deg.

Computer Resources

The initial computations were carried out on the Ballistic Research Laboratory CDC 7600 computer. This machine has a maximum large core storage capability of approximately 380,000 useable words. This limited the maximum computational grid to 21,600 points (60 longitudinal, 20 normal, and 18 circumferential). As previously mentioned, the solution is marched in time until a steady-state condition is obtained. A typical converged solution required approximately 1000 time steps. The CDC computation ran at a speed of 12.96×10^{-4} s/time step/point. This resulted in 7.78 h of computation time for one converged solution at one set of conditions. As will be shown later, this computational grid did not provide adequate grid resolution. This grid limitation problem has also been identified by Klopfer and Chaussee[13] who, using a symmetry version of an Euler code, found the minimum number of points required in the circumferential direction for adequate resolution to be 24.

In order to obtain improved grid resolution and faster computational speed, the computer code was placed on a remote Cray 1S computer. Operationally, the connection to the Cray was made via the MILNET (formerly ARPANET). MILNET is a Department of Defense digital switching network which allows terminals and geographically separated computers to communicate. The Cray 1S computer is a vector processor and has a demonstrated speed advantage over the CDC 7600 of 10 or more in the vector mode. The present computations, however, did not take full advantage of the vector capability. The same computation described earlier ran at a speed of 5.2×10^{-4} s/time step/point on the Cray which resulted in a 2.5 increase in speed for the same grid. An additional advantage in using the Cray was the increased storage capability. The Cray machine memory of 1 million words (860K useable) allowed the computational grid to be increased to 51,840 grid points (60 longitudinal, 24 normal, and 36 circumferential). It was felt that increased grid resolu-

tion in the circumferential direction was required for better resolution of the Magnus force components. The converged solution required 7.5 h on the Cray. With full vectorization, it is anticipated that this time can be reduced to 1.5 h. With the advent of even faster machines (Cray 2, with 256 million words of storage and speeds 6-12 times faster than the Cray 1) the eventual computational time potentially can be reduced to 15 min.

Results

The results to be presented are in the form of pressure coefficients, velocity profiles, and aerodynamic coefficients. All computed results are for $M=0.91$, $\alpha=2$ deg, and $Re=4.5\times10^6$, and a nondimensional spin rate of $PD/V=0.39$. The experimental data used for the comparison were obtained from two separate wind tunnel tests. Surface pressure data for a nonspinning configuration were obtained at NASA Langley.[11] The aerodynamic coefficient data for the spinning configuration were obtained at the Naval Surface Weapons Center.[12]

Surface Pressure Coefficient

The surface pressure coefficient C_p on the leeward ray is shown as a function of longitudinal position in Fig 5. The experimental data and computational results from both the CDC 7600 and Cray 1S computers are shown. The CDC results (dashed line) show marginal agreement with the experimental data (circles) over the entire projectile surface. The expansions and recompressions which occur near the ogive-cylinder and cylinder-boattail junctions have not been captured adequately by the computation. The solid line in Fig. 5 is the result from the computation on the Cray 1S computer where the grid has been refined. The agreement with the experimental data has improved significantly. Some discrepancy is still apparent, however, on the cylinder and boattail. As can be seen from Fig. 3, the grid points in the vicinity of the boattail have been severely stretched and is the apparent cause of the discrepancy. All remaining results to be presented were obtained from the Cray 1S. A comparison of the windward and leeward pressure distribution is shown in Fig. 6. The ogive experiences high pressure along the windward side, whereas the high pressure for the boattail is on the leeward side. This condition results in a couple about the center of gravity and contributes to the critical aerodynamic behavior that occurs at transonic velocities.

Comparisons between computation and experiment for the circumferential surface pressure distribution are shown in Figs. 7 and 8 for X/D stations 1.56 and 5.19, respectively. The experimental data are symmetric since they were obtained for a nonspinning configuration. As seen in these figures, the computation predicts the correct trend of the data, while the actual magnitude shows a deviation. A slight asymmetry is apparent in the computed circumferential pressure distribution near the $\phi=180$-deg plane. In this case, a small angle of attack was used and the asymmetry in the circumferential pressure distribution was expected to be small. This small asymmetry is the primary contribution to the Magnus (side) force. The grid used for these calculations is by no means optimum and additional computational experimentation is required. The results do, however, indicate the potential for obtaining satisfactory aerodynamic coefficients. This optimism is based on results obtained previously[5] for an axisymmetric computation. Figure 9 shows a comparison between experimental data and a computation using a grid with 80 longitudinal points and 40 points in the near-normal direction. The agreement is excellent and indicates the quality of results which should be possible for the three-dimensional cases when adequate grid resolution is achieved.

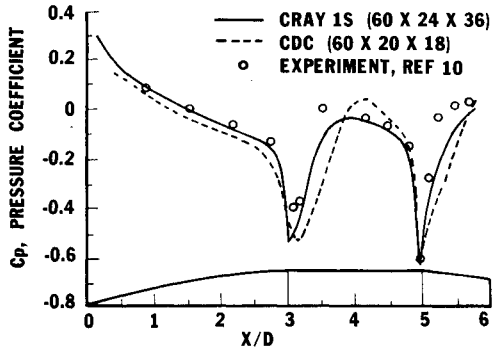

Fig. 5 Surface pressure coefficient, experiment and computations; $M=0.91$, $\alpha=2$ deg.

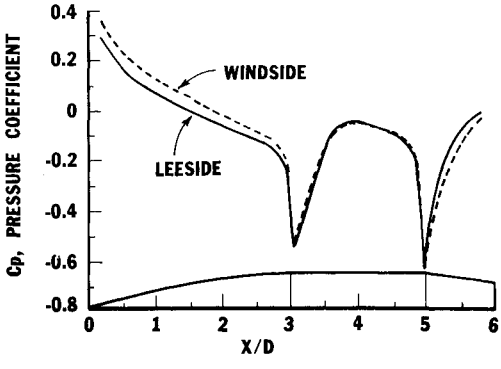

Fig. 6 Windward and leeward surface pressure coefficient; $M=0.91$, $\alpha=2$ deg.

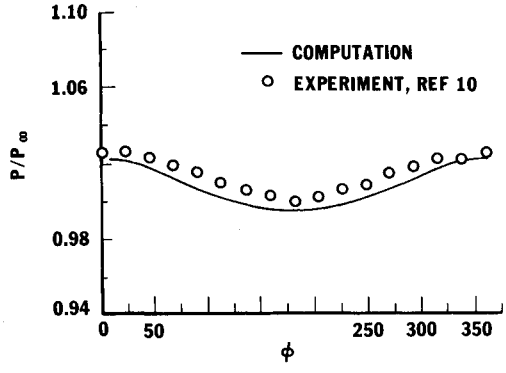

Fig. 7 Circumferential pressure distribution; $M=0.91$, $\alpha=2$ deg, $X/D=1.56$.

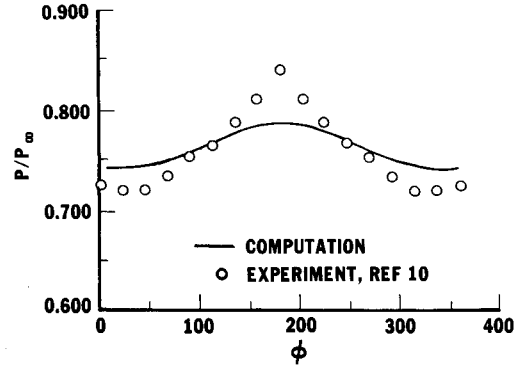

Fig. 8 Circumferential pressure distribution; $M=0.91$, $\alpha=2$ deg, $X/D=5.19$.

A primary purpose of this research effort is the development of a capability for the prediction of aerodynamic coefficients and, in particular, the capability to compute the Magnus effect. As noted, the Magnus effect is a viscous phenomenon associated with the spinning projectile. Therefore, in order for a computational technique to predict this effect, it must compute the longitudinal and circumferential wall shear stress adequately for the spinning projectile at angle of attack. The experimental determination of the u, v, and w velocity distributions is especially difficult at transonic velocities. Although no experimental data are available for comparison, the computed circumferential velocity distributions are shown in Figs. 10 and 11 for $X/D = 4.22$ and 5.50, respectively. A significant asymmetry can be seen in the velocity distributions at $\phi = 90$ and 270 deg. At $\phi = 90$ deg, cross-flow velocity caused by the angle of attack is in the same direction as the wall velocity. At $\phi = 270$ deg, the outer cross-flow opposes the wall velocity. The circumferential velocity profiles at $\phi = 0$ and 180 deg are equally affected by the surface spin. Figure 11 shows the velocity distribution at a station midway on the boattail. The circumferential velocity distribution at $\phi = 90$ and 270 deg has changed significantly from that shown in Fig. 10. On the boattail, the decreasing body diameter results in the surface velocity decreasing in magnitude. However, the boundary-layer thickness in this region increases and the effect of surface spin is seen to persist further out.

Pitch Plane and Magnus Coefficients

An integration of the pressure and viscous forces has been carried out to determine the aerodynamic coefficients. The sign convention used for the coefficients is shown in Fig. 12. The aerodynamic coefficients in Figs. 13-17 are plotted as a function of longitudinal position and illustrate the development of the force over the length of the projectile. Figure 13 is a plot of the normal force coefficient. The rapid increase in normal force that occurs on the ogive portion of the projectile is shown. The cylinder portion should produce no significant additional normal force; however, the computation indicates a slight increase in the normal force. The reversal in the direction of the force on the boattail can be seen clearly as the accumulated normal force coefficient, indicated by the circle, shows very good agreement with the computation.

As mentioned previously, the Magnus effect results from a spin-induced distortion of the viscous boundary layer which

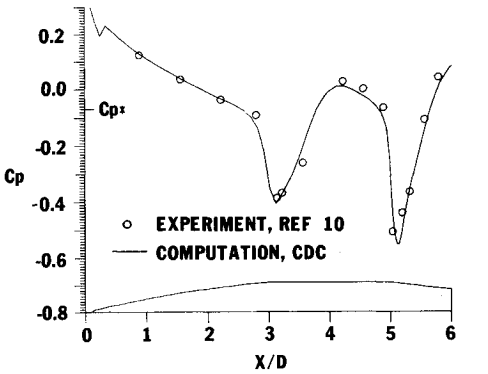

Fig. 9 Surface pressure coefficient, experiment and axisymmetric computation; $M = 0.96$, $\alpha = 0$ deg.

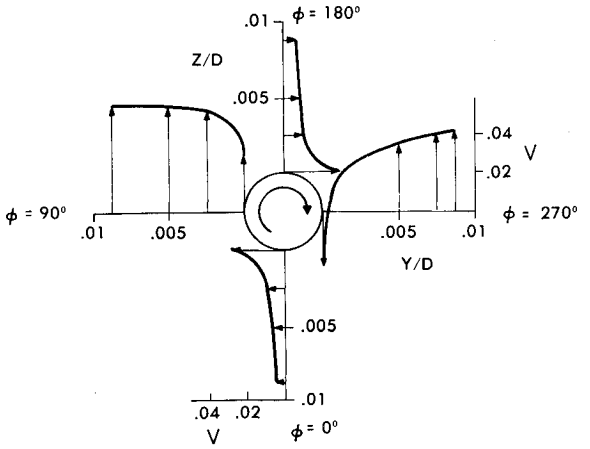

Fig. 10 Circumferential velocity profiles for $\phi = 0$, 90, 180, and 270 deg at $M = 0.91$, $\alpha = 2$ deg, $X/D = 4.22$, $PD/V = 0.39$.

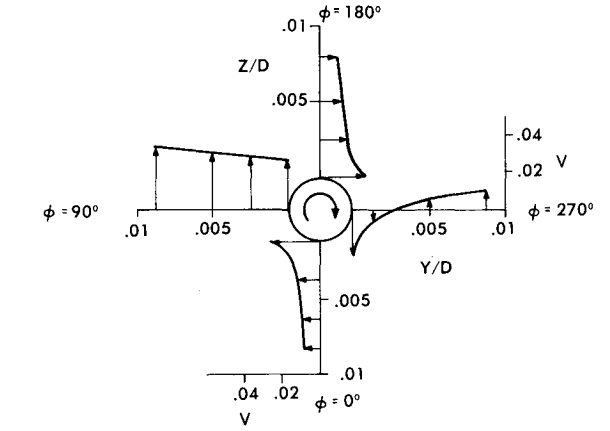

Fig. 11 Circumferential velocity profiles for $\phi = 0$, 90, 180, and 270 deg at $M = 0.91$, $\alpha = 2$ deg, $X/D = 5.5$, $PD/V = 0.39$.

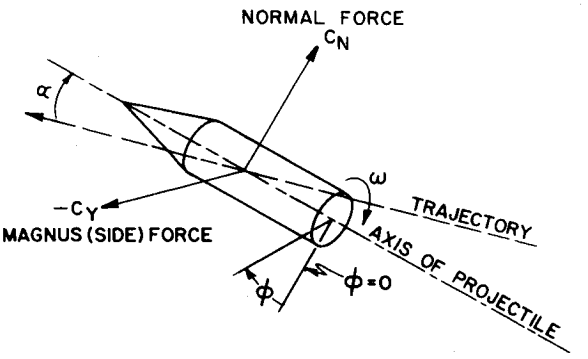

Fig. 12 Aerodynamic coefficient sign convention.

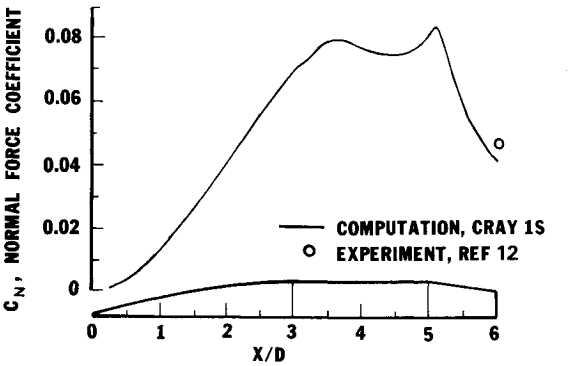

Fig. 13 Normal force coefficient along the projectile, computation and experiment; $M = 0.91$, $\alpha = 2$ deg.

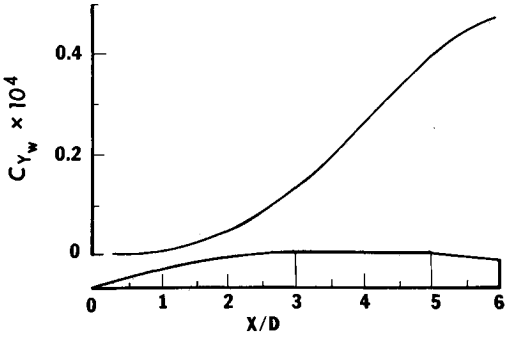

Fig. 14 Circumferential wall shear contribution to Magnus force; $M=0.91$, $\alpha=2$ deg, $PD/V=0.39$.

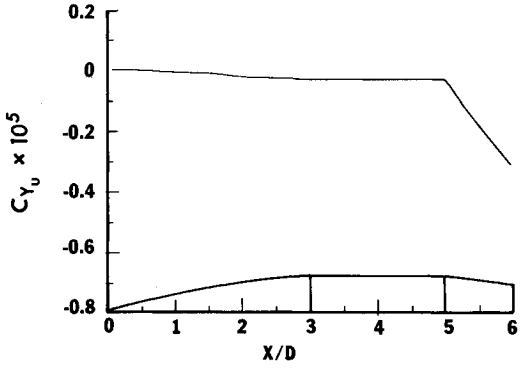

Fig. 15 Longitudinal wall shear contribution to the Magnus force; $M=0.91$, $\alpha=2$ deg, $PD/V=0.39$.

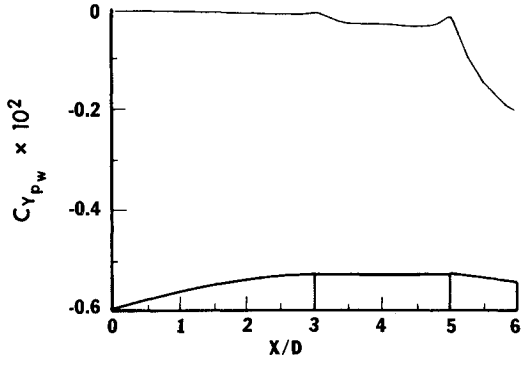

Fig. 16 Pressure contribution to the Magnus force; $M=0.91$, $\alpha=2$ deg, $PD/V=0.39$.

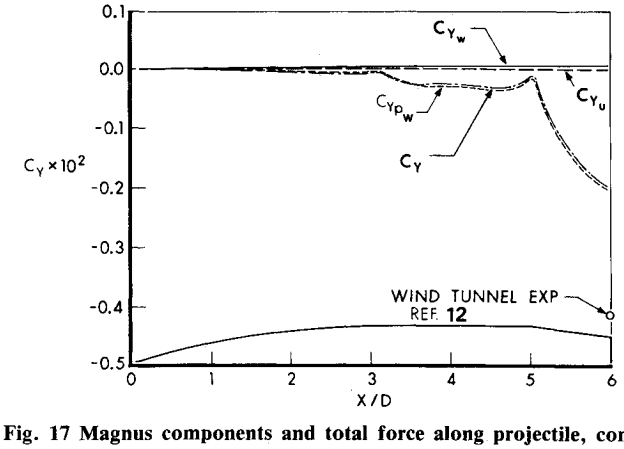

Fig. 17 Magnus components and total force along projectile, computation and experiment; $M=0.91$, $\alpha=2$ deg, $PD/V=0.39$.

occurs for a spinning shell at angle of attack. Previous studies[1,3] have shown that the Magnus effect consists of the sum of the boundary-layer displacement effect (asymmetric surface pressure distribution) plus the viscous wall shear stress contributions $\tau_x=\mu(du/dy)_{y=0}$ and $\tau_\phi=\mu(dw/dy)_{y=0}$. The development of all three components of the Magnus force are shown in Figs. 14, 15, and 16, respectively, as a function of longitudinal position. The longitudinal and circumferential components (Figs. 14 and 15) are seen to be on the order of 10^{-5} and 10^{-4}, respectively. The pressure component (Fig. 16) is on the order of 10^{-2}. The dominant component of the transonic Magnus effect is, therefore, seen to be the integration of the surface pressure, $C_{Y_{pw}}$. In addition, the largest portion of the total Magnus effect is seen to develop on the boattail where the viscous boundary layer reaches its maximum thickness. This is the same qualitative behavior reported by Sturek et al.[1,3] for supersonic flow. The total Magnus force C_Y and its components C_{Y_μ} (longitudinal shear stress), C_{Y_w} (circumferential shear stress), and $C_{Y_{pw}}$ (pressure) are shown in Fig. 17. The total Magnus force can be compared with the experimental force measurement. The individual components show their relative magnitude. Considering the small magnitude of the Magnus force and the agreement achieved for the normal force, the quantitative agreement between the computation and experiment is regarded as encouraging. The experimental Magnus force measurements were obtained in a wind tunnel not specifically designed for transonic flow and are considered to be of good qualitative value, but questionable quantitative value. Additional computations at various transonic Mach numbers and reliable experimental data are required before a full assessment of the computational technique can be made. Recently, experimental pressure data on a spinning projectile have been obtained by Miller.[14] Additional computations for this case are currently in progress. This first result, however, for predicting the Magnus effect at transonic velocity is considered very encouraging.

Summary

The research effort presented in this paper is part of an overall program to develop a sophisticated predictive capability for projectile aerodynamics. The pacing requirement for this capability is the determination of the Magnus force in the transonic flight regime.

An implicit finite difference code, which solves the unsteady thin-layer Navier-Stokes equations, has been applied to a projectile shape at $M=0.91$, $\alpha=2$ deg. The solution was marched in time until a steady-state result was obtained. Computations were first performed on a CDC 7600 using a finite difference grid of 21,600 points and required 7.78 h of computer time. Increased grid resolution with faster computational speed per grid point was obtained by performing the computation on a Cray 1S vector computer.

The circumferential velocity distribution, presented for two axial locations, showed a significant interaction between the primary cross-flow velocity and the body surface velocity. The computations have been compared to experimental measurements of surface pressure and aerodynamic forces. The normal force coefficient has been shown to be in good quantitative agreement with experimental data. The comparison for the Magnus force is considered fair. In addition, the individual components of the Magnus force have been presented and indicate qualitatively good results. The need for additional grid resolution has been identified as a further requirement to achieve more accurate predictions. Good-quality experimental data at transonic velocities are required for a more comprehensive code validation.

The present results indicate that the thin-layer Navier-Stokes computational technique, in conjunction with enhanced computer technology, has the potential of providing the capability to accurately predict the aerodynamic behavior of spinning shell at transonic velocities.

Acknowledgments

The cooperation and help from Dr. Wilbur Hankey and Mr. Jeff Graham, Air Force Wright Aeronautical Laboratories, Flight Dynamics Laboratory, Wright Patterson Air Force Base, Ohio, in initially using the Cray computer at Kirtland Air Force Base, New Mexico, is greatly appreciated.

References

[1]Sturek, W. B., Dwyer, H. A., Kayser, L. D., Nietubicz, C. J., Reklis, R. P., and Opalka, K. O., "Computations of Magnus Effects for a Yawed, Spinning Body of Revolution," *AIAA Journal,* Vol. 16, July 1978, pp. 687-692.

[2]Schiff, L. B. and Sturek, W. B., "Numerical Simulation of Steady Supersonic Flow Over Cone Ogive-Cylinder-Boattail Body," AIAA Paper 80-0066, Jan. 1980; also, ARBRL-TR-02363, Sept. 1981.

[3]Sturek, W. B. and Schiff, L. B., "Computations of the Magnus Effect for Slender Bodies in Supersonic Flow," *AIAA Journal,* Vol. 20, Dec. 1982, pp. 1724-1731.

[4]Nietubicz, C. J., Pulliam, T. H., and Steger, J. L., "Numerical Solution of the Azimuthal-Invariant Thin-Layer Navier-Stokes Equations,' *AIAA Journal,* Vol. 18, Dec. 1980, pp. 1411-1412.

[5]Nietubicz, C. J., "Navier-Stokes Computations for Conventional and Hollow Projectile Shapes at Transonic Velocities," AIAA Paper 81-1262, 1981; also, ARBRL-MR-03184, July 1982.

[6]Deiwert, G. S., "Numerical Simulation of Three Dimensional Boattail Afterbody Flow Field," *AIAA Journal,* Vol. 19, May 1981, pp. 582-588.

[7]Baldwin, B. S. and Lomax, H., "Thin Layer Approximation and Algebraic Model for Separated Turbulent Flows," AIAA Paper 78-257, Jan. 1978.

[8]Pulliam, T. H. and Steger, J. L., "On Implicit Finite-Difference Simulations of Three-Dimensional Flow," *AIAA Journal,* Vol. 18, Feb. 1980, pp. 159-167.

[9]Nietubicz, C. J., Heavey, K., and Steger, J., "Grid Generation Techniques for Projectile Configurations," *Proceedings of the 1982 Army Numerical Analysis and Computers Conference,* ARO Rept. 82-3, Feb. 1982, pp. 99-121.

[10]Beam, R. and Warming, R. F., "An Implicit Factored Scheme for the Compressible Navier-Stokes Equations," *AIAA Journal,* Vol. 16, April 1978, pp. 393-402.

[11]Kayser, L. D. and Whiton, F., "Surface Pressure Measurements on a Boattailed Projectile Shape at Transonic Speeds," ARBRL-MR-03161, March 1982.

[12]Kayser, L. D., unpublished wind tunnel data, Ballistic Research Laboratory, Aberdeen Proving Ground, Md., 1976.

[13]Klopfer, G. H. and Chaussee, D. S., "Numerical Solution of Three-Dimensional Transonic Flows Around Axisymmetric Bodies at Angle of Attack," 11th Navy Symposium on Aeroballistics, Philadelphia, Pa., Aug. 1978.

[14]Miller, M. C., "Surface Pressure Measurements on a Transonic Spinning Projectile," *Journal of Spacecraft and Rockets,* Vol. 22, March-April 1985, pp. 112-118.